

# Non-linear Hall effect in three-dimensional Weyl and Dirac semimetals

O.O. Shvetsov,<sup>1</sup> V.D. Esin,<sup>1</sup> A.V. Timonina,<sup>1</sup> N.N. Kolesnikov,<sup>1</sup> and E.V. Deviatov<sup>1</sup>

<sup>1</sup>*Institute of Solid State Physics of the Russian Academy of Sciences, Chernogolovka, Moscow District, 2 Academician Ossipyan str., 142432 Russia*

(Dated: February 11, 2019)

We experimentally investigate a non-linear Hall effect for three-dimensional  $\text{WTe}_2$  and  $\text{Cd}_3\text{As}_2$  single crystals, representing Weyl and Dirac semimetals, respectively. We observe finite second-harmonic Hall voltage, which depends quadratically on the longitudinal current in zero magnetic field. Despite this observation well corresponds to the theoretical predictions, only magnetic field dependence allows to distinguish the non-linear Hall effect from a thermoelectric response. We demonstrate that second-harmonic Hall voltage shows odd-type dependence on the direction of the magnetic field, which is a strong argument in favor of current-magnetization effects. In contrast, one order of magnitude higher thermopower signal is independent of the magnetic field direction.

PACS numbers: 73.40.Qv 71.30.+h

## I. INTRODUCTION

Non-linear Hall effect has been predicted in a wide class of time-reversal invariant materials<sup>1–5</sup>. In the linear response, there is no Hall current in the presence of time-reversal symmetry. It is argued in Refs. 1–5, that a non-linear Hall-like current can arise from the Berry curvature in momentum space. Since Berry curvature often concentrates in regions where two or more bands cross, three classes of candidate materials have been proposed<sup>4</sup>: topological crystalline insulators, two-dimensional transition metal dichalcogenides, and three-dimensional Weyl and Dirac semimetals. Another possible contribution to non-linear Hall effect is skew scattering with nonmagnetic impurities in time-reversal-invariant noncentrosymmetric materials<sup>6</sup>.

Recently, the time-reversal-invariant non-linear Hall (NLH) effect has been reported for layered transition metal dichalcogenides<sup>7,8</sup>. It stimulates a search for the Berry curvature dipole induced NLH effect in three-dimensional crystals, where Dirac and Weyl semimetals<sup>9</sup> are excellent candidates, since there is symmetry-protected conic dispersion in the bulk spectrum<sup>10,11</sup>. This spectrum has been experimentally confirmed by angle-resolved photoemission spectroscopy (ARPES), e.g., for  $\text{Cd}_3\text{As}_2$  Dirac material<sup>12,13</sup>, and for  $\text{MoTe}_2$  and  $\text{WTe}_2$  type II Weyl semimetals<sup>9,14,15</sup>. Because of low symmetry,  $\text{MoTe}_2$  and  $\text{WTe}_2$  are advantageous<sup>4</sup> in a search for the NLH effect.

In the experiments<sup>7,8</sup> on two-dimensional  $\text{WTe}_2$ , the the second-harmonic Hall voltage depends quadratically on the longitudinal current. In the simplified picture, an a.c. excitation current generates sample magnetization, which leads to the anomalous Hall effect<sup>16</sup> in zero external magnetic field. The latter appears as the second-harmonic Hall voltage, the amplitude is proportional to the square of the bias current. On the other hand, topological materials are characterized by strong thermoelectric effects<sup>17,18</sup>, which also appear as a second-harmonic quadratic signal<sup>19,20</sup>. For this reason, it is important to experimentally distinguish between the Berry curvature

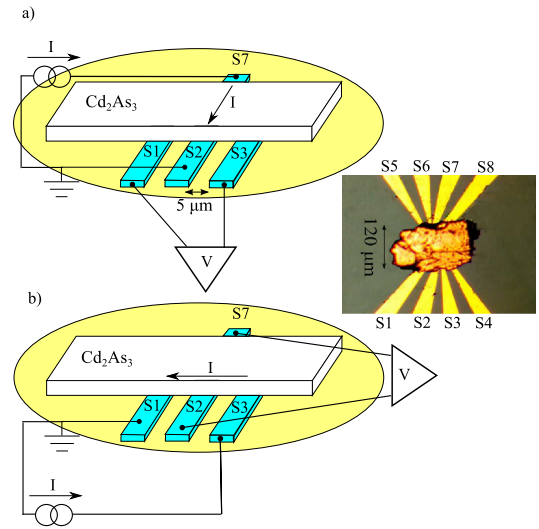


FIG. 1. (Color online) Top-view image of the sample with a small  $\text{Cd}_3\text{As}_2$  single crystal and the sketch with electrical connections. 100 nm thick and  $10\ \mu\text{m}$  wide Au leads are formed on a  $\text{SiO}_2$  substrate. A  $\text{Cd}_3\text{As}_2$  single crystal ( $\approx 100\ \mu\text{m}$  size) is transferred on top of the leads, forming contacts S1-S8 in regions of  $\approx 10\ \mu\text{m}$  overlap between the crystal and the leads. The second-harmonic ( $2\omega$ ) component of the Hall voltage  $V$  is investigated in a standard four-point lock-in technique in symmetric (a) and nonsymmetric (b) connection of the Hall voltage probes in respect to the current line (denoted by arrows), which mostly flows along the sample edge between S1 and S3 in the (b) case.

dipole induced NLH effect and a thermoelectric response while searching for the NLH effect in nonmagnetic materials.

Here, we experimentally investigate a non-linear Hall effect for three-dimensional  $\text{WTe}_2$  and  $\text{Cd}_3\text{As}_2$  single crystals, representing Weyl and Dirac semimetals, respectively. We observe finite second-harmonic Hall voltage, which depends quadratically on the longitudinal current in zero magnetic field. Despite this observation well corresponds to the theoretical predictions, only magnetic

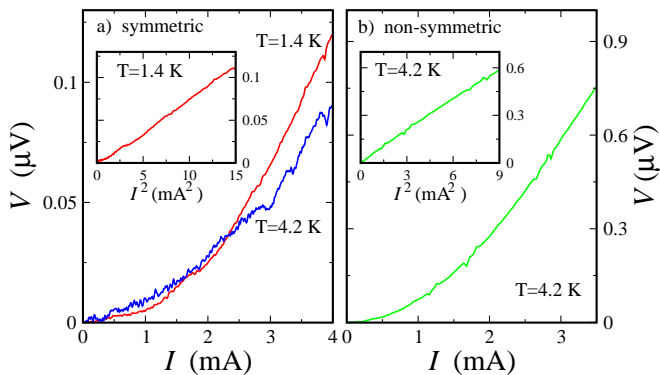


FIG. 2. (Color online) Examples of  $V(I)$  characteristics for a three-dimensional  $\text{Cd}_3\text{As}_2$  crystal. Here,  $V$  is the second-harmonic ( $2\omega$ )  $xy$  voltage component,  $I$  is the ac excitation current at frequency  $\omega$ . (a) In the case of the symmetric configuration, see Fig. 1 (a), the measured Hall voltage  $V$  is obviously non-linear,  $V \sim I^2$ , as it can be seen from the inset. The  $V(I)$  curve slightly (about 10%) depends on temperature in 1.4 K–4.2 K interval. (b) In the nonsymmetric configuration, depicted in Fig. 1 (b), the signal level is one order of magnitude higher, about  $1 \mu\text{V}$ , but the curve is still non-linear  $V \sim I^2$ , see the inset. The curves are obtained in zero magnetic field.

field dependence allows to distinguish the non-linear Hall effect from a thermoelectric response. We demonstrate that second-harmonic Hall voltage shows odd-type dependence on the direction of the magnetic field, which is a strong argument in favor of current-magnetization effects. In contrast, one order of magnitude higher thermopower signal is independent of the magnetic field direction.

## II. SAMPLES AND TECHNIQUE

$\text{Cd}_3\text{As}_2$  crystals were grown by crystallization of molten drops in the convective counterflow of argon held at 5 MPa pressure. For the source of drops the stalagmometer similar to one described<sup>21</sup> was applied. About one fifth of the drops were single crystals. The energy-dispersive X-ray spectroscopy (EDX) and X-ray powder diffractograms always confirmed pure  $\text{Cd}_3\text{As}_2$  with  $I4_1cd$  noncentrosymmetric group.

$\text{WTe}_2$  compound was synthesized from elements by reaction of metal with tellurium vapor in the sealed silica ampule. The  $\text{WTe}_2$  crystals were grown by the two-stage iodine transport<sup>22</sup>, that previously was successfully applied<sup>22,23</sup> for growth of other metal chalcogenides like  $\text{NbS}_2$  and  $\text{CrNb}_3\text{S}_6$ . The  $\text{WTe}_2$  composition is verified by EDX measurements. The X-ray diffraction confirms  $Pmn2_1$  orthorhombic single crystal  $\text{WTe}_2$ .

The initial  $\text{WTe}_2$  ingot is formed by a large number of small (less than  $100 \mu\text{m}$  size)  $\text{WTe}_2$  single crystals, which are weakly connected with each other. In contrast, small  $\text{Cd}_3\text{As}_2$  single crystals are obtained by a mechan-

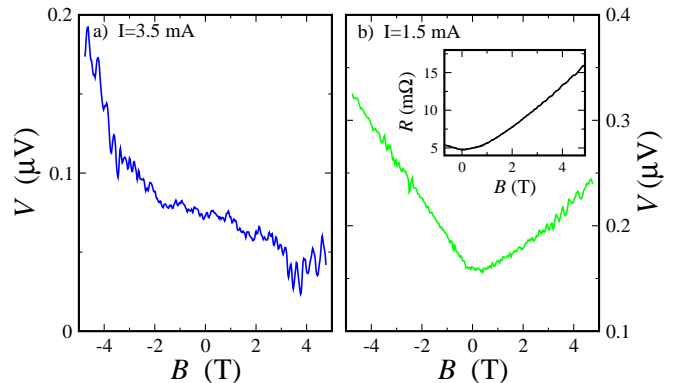


FIG. 3. (Color online) Second-harmonic voltage  $V$  dependence on the magnetic field  $B$  at fixed ac current  $I$  for three-dimensional  $\text{Cd}_3\text{As}_2$ . (a) In the case of the symmetric voltage probe configuration,  $\Delta V(B) = V(B) - V(B = 0)$  is nearly odd function, which is a strong argument in favor of current-magnetization effects. (b)  $V(B)$  increases for both field directions for the nonsymmetric connection scheme, which allows to identify the thermoelectric response. Inset demonstrates usual (first-harmonic)  $\text{Cd}_3\text{As}_2$   $xx$  magnetoresistance  $R(B)$  for our samples. All the curves are obtained at 4.2 K temperature.  $I = 1.5 \text{ mA}$  is diminishing for (b) with respect to the  $I = 3.5 \text{ mA}$  for (a), to avoid overheating effects for high signal in the (b) case.

ical cleaving method, somewhat similar to described in Ref. 24: we crush the initial 5 mm size  $\text{Cd}_3\text{As}_2$  drop onto small fragments. This procedure allows to create a clean  $\text{Cd}_3\text{As}_2$  surface without mechanical polishing or chemical treatment, see Ref. 25 for details.

Fig. 1 shows a top-view image of a sample. The leads pattern is formed by lift-off technique after thermal evaporation of 100 nm Au on the insulating  $\text{SiO}_2$  substrate. The  $10 \mu\text{m}$  wide Au leads are separated by  $5 \mu\text{m}$  intervals, see Fig. 1. Then, a small (about  $100 \mu\text{m}$  size)  $\text{Cd}_3\text{As}_2$  or  $\text{WTe}_2$  crystal is transferred to the Au leads pattern and pressed slightly with another oxidized silicon substrate. A special metallic frame allows to keep substrates parallel and apply a weak pressure to the piece. No external pressure is needed for a crystal to hold on a substrate with Au leads afterward.

We check by standard magnetoresistance measurements that our  $\text{Cd}_3\text{As}_2$  samples demonstrate large magnetoresistance with Shubnikov de Haas oscillations in high magnetic fields<sup>25</sup>. We estimate the concentration of carriers as  $n \approx 2.3 \times 10^{18} \text{ cm}^{-3}$  and low-temperature mobility as  $\mu \approx 10^6 \text{ cm}^2/\text{Vs}$ , which is in the good correspondence with known values<sup>26</sup>. Also, we check that our  $\text{WTe}_2$  samples demonstrate large, non-saturating positive magnetoresistance  $(\rho(B) - \rho(B = 0))/\rho(B = 0)$  in normal magnetic field, which goes to zero in parallel one, as it has been shown for  $\text{WTe}_2$  Weyl semimetal<sup>27</sup>. We do not see Shubnikov de Haas oscillations for  $\text{WTe}_2$  samples due to lower mobility, see Ref. 28 for details of magnetoresistance measurements. Examples of the magnetoresistance curves are also shown for our samples in the

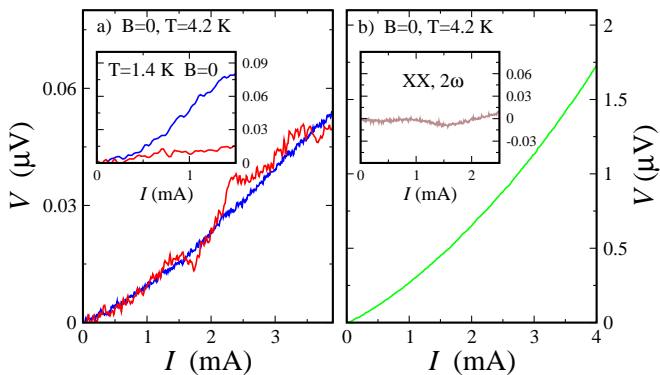


FIG. 4. (Color online) Examples of  $V(I)$  characteristics for a three-dimensional  $\text{WTe}_2$  crystal. Here,  $V$  is the second-harmonic ( $2\omega$ )  $xy$  voltage component,  $I$  is the ac excitation current at frequency  $\omega$ . (a) In the case of the symmetric configuration,  $V$  is nonlinear and is similar for the excitation current  $I$  along both  $a$  and  $b$  directions at 4.2 K. For lower (1.4 K) temperatures, the Hall voltage tends to zero for current along the  $a$  direction, as depicted in the inset. (b) Nonsymmetric connection leads to high (about  $1 \mu\text{V}$ ) nonlinear  $V \sim I^2$  Hall voltage. Inset to (b) demonstrates very small (below 10 nV) second-harmonic  $xx$  signal, i.e. for ac current flowing between S1 and S4, while the potential drop at  $2\omega$  is measured between S2 and S3 in Fig. 1. The curves are obtained in zero magnetic field.

insets to Figs. 3 and 5.

We measure the second-harmonic component of the Hall voltage in standard ac lock-in technique. To study NLH effect, the special care has been taken to ensure that the Hall probes are symmetric in respect to the current line, as depicted in Fig. 1 (a): the ac current flows between contacts S2 and S7, while the Hall voltage is measured between two neighbour contacts S1 and S3. In this symmetric configuration, there is no temperature gradients between the potential probes, which allows to exclude thermoelectric effects. The latter should be dominant in the nonsymmetric configuration, see Fig. 1 (b), where the current flows between S1 and S3 along the sample edge, while the potential drop is measured across the sample between S2 and S7.

We ensure, that the measured voltage is antisymmetric with respect to the voltage probe swap and it is independent of the ground probe position. We check, that the lock-in signal is also independent of the modulation frequency (about 110 Hz). The measurements are performed in a standard 1.4 K–4.2 K cryostat equipped with superconducting solenoid.

### III. EXPERIMENTAL RESULTS

Examples of  $I - V$  characteristics are shown in Fig. 2 for symmetric (a) and nonsymmetric (b) configurations of the voltage probes. In the case of the symmetric configuration, like depicted in Fig. 1 (a), we obtain clearly

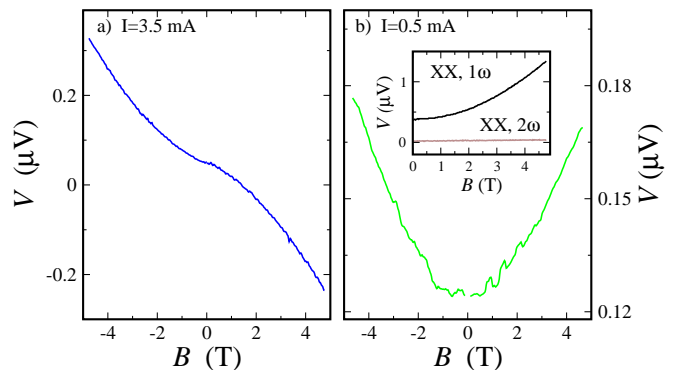


FIG. 5. (Color online) Second-harmonic voltage  $V$  dependence on the magnetic field  $B$  at fixed ac current  $I$  for three-dimensional  $\text{WTe}_2$ . (a) In the case of the symmetric voltage probe configuration,  $\Delta V(B) = V(B) - V(B = 0)$  is the odd function of  $B$ , similarly to the  $\text{Cd}_3\text{As}_2$  case. (b)  $V(B)$  is nearly even function for the nonsymmetric connection scheme.  $I = 0.5 \text{ mA}$  is diminishing for (b) with respect to the  $I = 3.5 \text{ mA}$  for (a), to avoid overheating effects for high signal in (b) case. Inset to (b) demonstrates usual (first-harmonic)  $\text{WTe}_2$   $xx$  magnetoresistance for our samples and nearly zero second-harmonic  $xx$  component. The curves are obtained at 4.2 K temperature.

non-zero Hall voltage  $V^{2\omega}$  for the second harmonics of the ac excitation current  $I$ . The measured  $V^{2\omega}$  is below  $0.1 \mu\text{V}$ , it slightly (about 10%) depends on temperature in 1.4 K–4.2 K interval. The  $I - V$  curve is obviously non-linear,  $V^{2\omega} \sim I^2$ , as it can be seen from the inset to Fig. 2 (a).

This behavior well corresponds<sup>7,8</sup> to the expected<sup>1,3–5</sup> for NLH effect. However, this interpretation can not be accepted without additional arguments. For example, if the potential contacts are not symmetric in respect to the current line, see Fig. 1 (b), we also obtain non-linear,  $V^{2\omega} \sim I^2$ ,  $I - V$  curve, as presented in Fig. 2 (b). In this case the signal level is one order of magnitude higher, about  $1 \mu\text{V}$ , which better corresponds to typical thermopower values<sup>18</sup>.

To experimentally determine the origin of the effect in every of these two cases, we apply an external magnetic field. Fig. 3 demonstrates second-harmonic voltage dependence on the magnetic field  $V^{2\omega}(B)$  at fixed ac current values. In the case of the symmetric configuration, see Fig. 3 (a),  $\Delta V^{2\omega}(B) = V^{2\omega}(B) - V^{2\omega}(B = 0)$  is nearly odd function, i.e.  $V^{2\omega}(B)$  depends on the magnetic field direction:  $V^{2\omega}(B)$  is diminishing for the positive fields, while it is increasing for the negative ones. In contrast,  $V^{2\omega}(B)$  increases for both field directions for the nonsymmetric connection scheme, see Fig. 3 (b). In this case,  $V^{2\omega}(B)$  even quantitatively resembles  $\text{Cd}_3\text{As}_2$  magnetoresistance<sup>25</sup>, which is depicted in the inset to Fig. 3 (b) for our samples.

The observed behavior can be reproduced not only for different samples in different cooling cycles, but also can be demonstrated for another three-dimensional material,

like WTe<sub>2</sub> Weyl semimetal, see Figs. 4 and 5.

The measured nonlinear second-harmonic Hall voltage  $V^{2\omega}$  is also below 0.1  $\mu\text{V}$  for the symmetric Hall probe connection scheme. Like for Cd<sub>3</sub>As<sub>2</sub> samples, nonsymmetric connection leads to high (about 1  $\mu\text{V}$ ) nonlinear  $V^{2\omega} \sim I^2$  voltage, see Fig. 4 (b). We also check, that there is no significant second-harmonic signal for the voltage probes situated along the current line, i.e.  $xx$  voltage component is below 10 nV, see the inset to Fig. 4 (b).

The specifics of NLH effects for layered WTe<sub>2</sub> is the strong signal dependence on the current direction<sup>7,8</sup>. In our case of three-dimensional WTe<sub>2</sub>, we obtain nearly the same  $V^{2\omega}$  for currents along both  $a$  and  $b$  directions at the liquid helium temperature 4 K, see Fig. 4 (a). For lower (1.4 K) temperatures, the Hall voltage  $V^{2\omega}$  tends to zero for current along the  $a$  direction, as depicted in the inset to Fig. 4 (a). This is the difference of our  $I - V$  curves from the layered two-dimensional WTe<sub>2</sub>, where there was no strong temperature dependence<sup>7,8</sup>.

The similarity between Cd<sub>3</sub>As<sub>2</sub> and WTe<sub>2</sub> crystals can also be seen in the magnetic field behavior, see Fig. 5. For the symmetric connection scheme,  $V^{2\omega}(B)$  demonstrates strong odd-type behavior in respect to the magnetic field direction, as demonstrated in the (a) panel. In contrast,  $V^{2\omega}(B)$  is clearly even-type in Fig. 5 (b), which well corresponds to the bulk WTe<sub>2</sub> non-saturating  $xx$  magnetoresistance<sup>27</sup>, see the inset to the panel (b). We wish to note, that there is no noticeable field dependence for the second-harmonic ( $2\omega$ )  $xx$  tensor component, see also the inset to Fig. 5.

#### IV. DISCUSSION

As a result, we obtain non-linear second-harmonic  $xy$  signal  $V^{2\omega} \sim I^2$ , which demonstrates different magnetic field behavior, even- or odd-type, for nonsymmetric or strictly symmetric configurations of voltage probes, respectively.

The odd  $V^{2\omega}(B)$  dependence is a good argument for NLH origin of the non-zero second-harmonic Hall voltage: if the ac excitation current generates sample magnetization, the latter should be sensitive to the direction of external magnetic field. More precisely, it is possible to demonstrate<sup>29</sup> from the kinetic equation (in the spirit of Ref. 4), that second - order response is absent in classical Hall effect, while it is an odd function of magnetic field for the spectrum with Berry curvature (Weyl semimetals).

In contrast, thermoelectric effects are defined by the sample heating, which is proportional to  $RI^2$  in our case, i.e. they also produce the second-harmonic response. The magnetic field dependence should be mainly defined by the magnetoresistance  $R(B)$ , since it is extremely strong in Weyl and Dirac semimetals. Thus, the thermoelectric response can not be sensitive to the magnetic field direction. In the experiment,  $V^{2\omega}(B)$  even quantitatively resembles  $R(B)$  magnetoresistance, see Figs. 3

and 5 for our samples. Note, that Nernst effect can not contribute to the measured  $xy$  voltage, since the temperature gradient is along the  $y$  axis in the geometry of the experiment. On the other hand, the Seebeck effect is also characterized<sup>30</sup> by even,  $R(B)$ -like magnetic field dependence.

Thus, we can identify high second-harmonic signal as thermoelectric voltage for nonsymmetric connection schemes, while low  $V^{2\omega}$  reflects NLH effect for the strictly symmetric ones.

For both connection schemes, some admixture of the effects is possible. We can not completely avoid an asymmetry of the potential contacts, so an admixture of  $R(B)$  produces distortions in high fields in Fig. 3 (a). On the other hand, NLH effect should be present also in the nonsymmetric connection scheme, where the thermoelectric response dominates. Due to the strong odd field dependence of NLH voltage, it can be responsible for the observed  $V^{2\omega}$  branch asymmetry in Figs. 3 (b) and 5 (b).

While NLH effect was originally proposed<sup>4</sup> for Weyl and Dirac semimetals, it can only be seen for noncentrosymmetric crystals. This requirement is obviously fulfilled for the type II Weyl semimetal WTe<sub>2</sub>, but there is a discussion in the case of Cd<sub>3</sub>As<sub>2</sub>. Ref. 31 insists on the near-centrosymmetric structure with the space group  $I4_1/acd$ . On the other hand, the previously established<sup>32</sup>  $I4_1cd$  noncentrosymmetric group is also confirmed in recent investigations<sup>33</sup> and this crystal symmetry is in a reasonable correspondence with ARPES data on the Cd<sub>3</sub>As<sub>2</sub> electronic structure<sup>33</sup>. This difference should originate from the Cd<sub>3</sub>As<sub>2</sub> growth method, e.g. the X-ray diffraction confirms  $I4_1cd$  noncentrosymmetric group for our samples. Also, in our case, strain may occur at SiO<sub>2</sub>-Cd<sub>3</sub>As<sub>2</sub> interface due to materials misfit, which affects the initial symmetry<sup>34</sup>. It is worth mentioning, that skew scattering is allowed in all noncentrosymmetric crystals, whereas Berry curvature dipole requires more strict symmetry conditions<sup>6</sup>. We still can not distinguish these two contributions to NLH effect in the present experiment.

#### V. CONCLUSION

We experimentally investigate a non-linear Hall effect for three-dimensional WTe<sub>2</sub> and Cd<sub>3</sub>As<sub>2</sub> single crystals, representing Weyl and Dirac semimetals, respectively. We demonstrate finite second-harmonic Hall voltage, which depends quadratically on the longitudinal current in zero magnetic field. If the potential contact are perfectly symmetric in respect to the current line, the observed signal is in the nanovolt range. It shows odd-type dependence on the direction of the magnetic field, which is a strong argument in favor of current-magnetization effects. If the potential contact are strongly nonsymmetric, temperature gradient produces one order of magnitude higher thermopower signal with even-type magnetic field dependence.

## ACKNOWLEDGMENTS

We wish to thank Leonid E. Golub, Yu.S. Barash, and V.T. Dolgoplov for fruitful discussions. We gratefully

acknowledge financial support partially by the RFBR (project No. 19-02-00203), RAS, and RF State contracts.

- 
- <sup>1</sup> E. Deyo, L. E. Golub, E. L. Ivchenko, and B. Spivak, arXiv:0904.1917 (2009).
- <sup>2</sup> L.E. Golub, E.L. Ivchenko, B.Z. Spivak, JETP Letters, 105, 782 (2017)
- <sup>3</sup> J. E. Moore and J. Orenstein, Phys. Rev. Lett., 105, 026805 (2010).
- <sup>4</sup> Inti Sodemann and Liang Fu, Phys. Rev. Lett., 115, 216806 (2015).
- <sup>5</sup> T. Low, Y. Jiang, and F. Guinea, Physical Review B 92, 235447 (2015).
- <sup>6</sup> Hiroki Isobe, Su-Yang Xu, Liang Fu, arXiv:1812.08162 (2018)
- <sup>7</sup> Kaifei Kang, Tingxin Li, Egon Sohn, Jie Shan, Kin Fai Mak, arXiv:1809.08744 (2018).
- <sup>8</sup> Qiong Ma, et al., arXiv:1809.09279 (2018).
- <sup>9</sup> As a recent review see N. P. Armitage, E. J. Mele, and A. Vishwanath, Rev. Mod. Phys. 90, 15001 (2018).
- <sup>10</sup> Z. Wang, H. Weng, Q. Wu, X. Dai, and Z. Fang, Phys. Rev. B **88**, 125427 (2013), 10.1103/physrevb.88.125427.
- <sup>11</sup> Z. Wang, Y. Sun, X.-Q. Chen, C. Franchini, G. Xu, H. Weng, X. Dai, and Z. Fang, Phys. Rev. B **85**, 195320 (2012), 10.1103/physrevb.85.195320.
- <sup>12</sup> Z. K. Liu, J. Jiang, B. Zhou, Z. J. Wang, Y. Zhang, H. M. Weng, D. Prabhakaran, S. K. Mo, H. Peng, P. Dudin, T. Kim, M. Hoesch, Z. Fang, X. Dai, Z. X. Shen, D. L. Feng, Z. Hussain, and Y. L. Chen, Nat. Mater. **13**, 677 (2014), 10.1038/nmat3990.
- <sup>13</sup> S. Borisenko, Q. Gibson, D. Evtushinsky, V. Zabolotnyy, B. Büchner, and R. J. Cava Phys. Rev. Lett. **113**, 027603 (2014), 10.1103/physrevlett.113.027603.
- <sup>14</sup> Ch. Wang, Y. Zhang, J. Huang, S. Nie, G. Liu, A. Liang, Yu. Zhang, B. Shen, J. Liu, C. Hu, Y. Ding, D. Liu, Y. Hu, S. He, L. Zhao, L. Yu, J. Hu, J. Wei, Z. Mao, Y. Shi, X. Jia, F. Zhang, S. Zhang, F. Yang, Z. Wang, Q. Peng, H. Weng, X. Dai, Z. Fang, Z. Xu, C. Chen, and X.J. Zhou, Phys. Rev. B **94**, 241119(R) (2016).
- <sup>15</sup> Y. Wu, D. Mou, N.H. Jo, K. Sun, L. Huang, S.L. Budko, P.C. Canfield, A. Kaminski, Phys. Rev. B **94**, 121113(R) (2016).
- <sup>16</sup> Nagaosa, N., Sinova, J., Onoda, S., MacDonald, A.H. and Ong, N.P. , Reviews of Modern Physics 82, 1539-1592 (2010).
- <sup>17</sup> C. Fu, Th. Scaffidi, J. Waissman, Y. Sun, R. Saha, S. J. Watzman, A. K. Srivastava, G. Li, W. Schnelle, P. Werner, M. E. Kamminga, S. Sachdev, S. S. P. Parkin, S. A. Hartnoll, C. Felser, J. Gooth, arXiv:1802.09468.
- <sup>18</sup> Tong Zhou, Cheng Zhang, Huisheng Zhang, Faxian Xiu, Zhongqin Yang, Inorg. Chem. Front., 3, 1637 (2016).
- <sup>19</sup> G.M. Gusev, O.E. Raichev, E.B. Olshanetsky, A.D. Levin, Z.D. Kvon, N.N. Mikhailov and S.A. Dvoretzky, 2D Mater., 6, 014001 (2019); E. B. Olshanetsky, Z. D. Kvon, M. V. Entin, L. I. Magarill, A. Levin, G. M. Gusev, N. N. Mikhailov, JETP Lett. 107, 789 (2018);
- <sup>20</sup> A. Mokashi, S. Li, B. Wen, S.V. Kravchenko, A.A. Shashkin, V.T. Dolgoplov, and M.P. Sarachik, Phys. Rev. Lett., 109, 096405 (2012)
- <sup>21</sup> N. N. Kolesnikov, M. P. Kulakov, Yu. N. Ivanov, J. Cryst. Growth **125**, 576 (1992).
- <sup>22</sup> E. B. Borisenko, V. A. Berezin, N. N. Kolesnikov, V. K. Gartman, D. V. Matveev, O. F. Shakhlevich, Physics of the Solid State, 59, 1310, (2017).
- <sup>23</sup> A. Sidorov, A.E. Petrova, A.N. Pinyagin, N.N. Kolesnikov, S.S. Khasanov, S.M. Stishov, JETP, 122, 1047, (2016).
- <sup>24</sup> W. Yu, W. Pan, D. L. Medlin, M. A. Rodriguez, S. R. Lee, Z. Bao, and F. Zhang, arXiv:1801.04364
- <sup>25</sup> O. O. Shvetsov, V. D. Esin, A. V. Timonina, N. N. Kolesnikov, E. V. Deviatov, arXiv:1811.02475
- <sup>26</sup> For a review on Cd<sub>3</sub>As<sub>2</sub> properties, see I. Crassee, R. Sankar, W.-L. Lee, A. Akrap, M. Orlita, arXiv:1810.03726
- <sup>27</sup> Mazhar N. Ali, Jun Xiong, Steven Flynn, Jing Tao, Quinn D. Gibson, Leslie M. Schoop, Tian Liang, Neel Hal- dolaarachchige, Max Hirschberger, N. P. Ong and R. J. Cava Nature 514, 205 (2014). doi:10.1038/nature13763
- <sup>28</sup> A. Kononov, O. O. Shvetsov, S. V. Egorov, A. V. Timonina, N. N. Kolesnikov and E. V. Deviatov EPL, 122, 27004 (2018) doi: 10.1209/0295-5075/122/27004
- <sup>29</sup> The calculation will be published elsewhere.
- <sup>30</sup> M.C. Steele, Physical Review, 107, 81 (1957).
- <sup>31</sup> Mazhar N. Ali, Quinn Gibson, Sangjun Jeon, Brian B. Zhou, Ali Yazdani, and R. J. Cava, Inorg. Chem., 53, 40624067 (2014) DOI: 10.1021/ic403163d
- <sup>32</sup> G. Steigmann, J. Goodyear, Acta Crystallogr., Sect. B: Struct. Crystallogr. Cryst. Chem., 24, 1062 (1968).
- <sup>33</sup> Hemian Yi, Zhijun Wang, Chaoyu Chen, Youguo Shi, Ya Feng, Aiji Liang, Zhuojin Xie, Shaolong He, Junfeng He, Yingying Peng, Xu Liu, Yan Liu, Lin Zhao, Guodong Liu, Xiaoli Dong, Jun Zhang, M. Nakatake, M. Arita, K. Shimada, H. Namatame, M. Taniguchi, Zuyan Xu, Chuangtian Chen, Xi Dai, Zhong Fang, X. J. Zhou, Scientific Reports 4, 6106 (2014)
- <sup>34</sup> E. Tang and L. Fu, Nature Phys. **10**, 964 (2014); arXiv:1403.7523.